SI appendix for: How selective severing by katanin promotes order in the plant cortical microtubule array

Eva E. Deinum [*] [†] [‡], **Simon H. Tindemans** [†] [§], **Jelmer J. Lindeboom** [¶] **and Bela M. Mulder** [†] [‖]

[*]Mathematical and Statistical Methods, Wageningen University & Research, 6708 PB Wageningen, The Netherlands, [†]Systems Biophysics, AMOLF, 1098XG Amsterdam, the Netherlands, [¶]Department of Plant Biology, Carnegie Institution for Science, Stanford CA 94305, USA, [‖]Laboratory of Cell Biology, Wageningen University & Research, 6708 PB Wageningen, the Netherlands, [§]Present address: Department of Electrical and Electronic Engineering, Imperial College London, London SW7 2AZ, United Kingdom, and [‡]To whom correspondence should be addressed. Email: eva.deinum@wur.nl

Edited by Olivier Hamant, École Normale Supérieure de Lyon, Lyon, France, and accepted by Editorial Board Member Caroline Dean May 9, 2017 (received for review February 24, 2017)

Supplementary text

T1 Unbiased selection of snapshots (fig. 1E)

To avoid a result driven bias in the selection of snapshots for the overview diagram of fig. 1E, we applied the following automated selection criterion. For each parameter combination, we obtained snapshots (after 30h of simulated time) for 5 independent simulations. Of these, we blindly selected one with median S_2 value of the five.

T2 Unstable alignment with aselective crossover severing and $P_{cat} = 0.09$

In our simulations with crossing-only severing and a low induced catastrophe probability ($P_{cat} = 0.09$), we observed that crossing-only severing could produce at best an intermediate degree of alignment (up to $S_2 \approx 0.4$).

To understand this intermediate degree of alignment we performed a number of extra long simulations of 100 hours (> 4 days). Fig. S3C,D,E shows time traces of the degree of alignment of several individual runs, colored by the overall orientation of the array, and some snapshots of the system of two runs, as indicated by arrows in fig. S3D. Strikingly, these runs do not show the usual pattern of a stable increase of S_2 until some plateau is reached [e.g. see fig. S6C,D and 1; 2], but several periods with intermediate S_2 separated by periods with very low S_2. We also observed that the net orientation of the array in consecutive aligned periods was often different. We noted that the arrays without severing looked similar to those in complete absence of induced catastrophes in that they could locally harbour up to four orientations differing by more than 40° [c.f. fig. S1 in 2], suggesting that with this low value of $P_{cat} = 0.09$, the effect of bundling is so distorting with respect to alignment that the induced catastrophes cannot overcome it (or perhaps only *very* close to $G_c = 0$ and with *very* long equilibration times).

With this implementation of crossover severing, either the crossed over or the crossing bundle is selected for a severing event with equal probability, regardless of the number of MTs in each bundle. In the – not necessarily realistic – regime that severing typically occurs so fast that the number of MTs at the crossover in both bundles remains otherwise unchanged, the expected number of crossed over MTs in a bundle of n that is severed before a single crossing one is $1 - (\frac{1}{2})^n$, which rapidly converges to 1. This calculation allows for the possibility that with low spontaneous catastrophe rates r_c, high crossover severing rates r_x and few/no induced catastrophes, there is a regime in which a single discordant MT is likely to cause multiple severing events of concordant MTs before undergoing an induced catastrophe itself. We hypothesize that this is the basis of the recurring decline of alignment in these systems. Biologically, this would suggest that increasing the fraction of severing events targeting crossed over MTs could aid in the breakdown of an established array orientation.

T3 MT length distributions

Exponential distributions in absence of severing. Early theoretical work on non-interacting MTs in absence of severing predicts an exponential length distribution [3]. This prediction is conserved for interacting MTs, even with bundling (but no severing) [4], which we readily confirmed in our simulations (fig. S2A).

More compact distributions with random severing. Theoretical work on non-interacting MTs predicts that random severing leads to more "compact" length distributions, i.e., with fewer long MTs than with an exponential distribution [5]. This happens because random severing occurs with a constant rate (r_s) per unit of MT length, so longer MTs are more likely to get severed somewhere. We also found these compact distributions in our interacting system (fig. S1). The effect was more pronounced with increasing severing rate r_s.

Crossing-only severing results in mostly exponential distributions. With bundling, when crossing-only severing is effective in promoting alignment, we found exponential length distributions (fig. S2B). We did not detect the compacting effect on the length distributions that we saw with random severing. This indicates that this form of severing is not randomly affecting all MTs, but preferentially affects discordant MTs with the same proportionality as induced catastrophes do. This observation thus supports our claim that crossing-only severing promotes alignment in a way similar to induced catastrophes (albeit less effective).

Reserved for Publication Footnotes

Local domain formation affects MT length distributions. It is possible that the system aligns, but forms multiple domains with distinct orientations [fig. 1E; see also 6; 2]. This, of course, interferes with the MT length distributions, for example see (fig. S2C). The distinct peaks in the histogram of the dominant orientation angles correlate with the length of individual domains appeared as peaks in the histogram.

"Mixed" length distributions in absence of bundling. Fig. S2D shows an example of length distributions with crossing-only severing and no bundling. The distributions appear as mixture of the compact distributions created by random severing, particularly for the discordant angles, and exponential, in the tails of the concordant angles, typical of no severing and crossing-only severing in the presence of bundling. In other words: at the concordant angles, all but the shortest length class show an exponential distribution, which indicates they are hardly affected by severing, whereas the other MTs follow a more compact distribution, suggesting severing is frequent among those. This effect occurs because new stretches of MT length are typically crossing at crossovers, and with increasing age, the likelihood of a stretch being the crossed over one increases and, hence, the exposure to severing decreases. Only concordant MTs are likely to get so old that severing ceases over most of their lattice, so the exponential tail is only expected for the majority orientation.

With bundling, on the other hand, concordant MTs are likely to entrain with older MTs soon after their nucleation, which increases their chances of being on an "old" bundle. This difference also explains that we found a larger aligned regime for crossing-only severing with bundling, than without bundling in combination with a protected angle of 40° or 60°.

T4 Increasing crossing-only severing rates make the width of the aligned regime (G^*) less dependent on the induced catastrophe probability (P_{cat})

The survival-of-the-aligned theory predicts that in absence of severing (and regardless of bundling) the width of the aligned regime increases with increasing induced catastrophe probability P_{cat} (i.e., G^* gets smaller). Adding crossing-only severing to the theory as a tunable weaker form of induced catastrophes () yields the prediction that with increasing crossover severing rates r_x, the width of the aligned regime becomes less dependent on P_{cat}. Considering all our simulations with bundling and crossing-only severing together supports that: the location of the onset of the aligned regime is almost the same at high values of r_x, but very different without severing (fig. 3), (all simulations with bundling; separately shown in figures 1D ($P_{cat} = 0.5$), S6A ($P_{cat} = 0.09$), and S7AB and S8AB ($P_{cat} = 0$)).

T5 Measuring length distributions of discordant MT populations

Length distributions were measured based on 100 independent simulations per parameter set. We used a 2D histogram of MT segment orientation (10 bins of 18°width) and length (20 bins). The bins for MT segment length were of equal size per orientation, but their width was adapted dynamically to the length of simulated MT segments: bin widths were scaled successively by a factor of two to accommodate the largest segment. During simulations, histograms were computed as averages of 5 measurements 3 minutes apart.

Observing maximum length of all histograms, we concluded that histograms with a maximum length of 8 μm or less always represented minority orientations, except when changing v^+, where a maximum length of 16 μm was needed. We averaged the MT segment counts of all these "short" histograms per parameter combination (so individual simulations could contribute more than one histogram). Where possible, we used both 8 μm and 16 μm as a maximum. The differences between both were small, and all trends and differences within and between groups were conserved (table S2).

To ensure the same value of $G_c = -0.121729$ for all values of v^t, we adjusted r_c as given below. All other parameters were default values.

v^t $(\mu m/s)$	r_c (s^{-1})	l_0 $(\mu m)^a$
0.01	0.00480707426531	36.4
0.02	0.00412714867275	33.4
0.03	0.0035	30.2
0.04	0.00291296245279	26.4
0.05	0.00235244248501	22.2
0.06	0.00179965165925	17.2

For varying r_r, the following r_c values were used for ensuring the same value of $G_c = -0.121282$

r_r (s^{-1})	r_c (s^{-1})	l_0 (μm)
0.003	0.00315294117647	36.5
0.005	0.00397647058824	36.5
0.007	0.0048	36.5
0.009	0.00562352941176	36.5
0.012	0.00685882352941	36.5

For varying v^+, the following r_c values were used for ensuring the same value of $G_c = -0.121282$. Moreover, the cutoff for the discordant MT orientations was a maximum length of 16 μm, because with the higher values of v^+, little/no shorter histograms occurred.

v^+ $(\mu m/s)$	r_c (s^{-1})	l_0 (μm)
0.05	0.00294838256325	30.7
0.08	0.0048	36.5
0.12	0.00721607300528	40.9
0.16	0.00960485355814	43.7

For varying v^-, the following r_c values were used for ensuring the same value of $G_c = -0.121282$.

v^- $(\mu m/s)$	r_c (s^{-1})	l_0 (μm)
0.08	0.00751525512526	33.8
0.12	0.00574260803081	35.5
0.16	0.0048	36.5
0.20	0.00421478969932	37.2
0.25	0.00373542367372	37.8

Fractions of short MTs are provided in table S2.

[a] l_0 is the theoretical average equilibrium length of non-interacting MTs:

$$l_0 = -1 \Big/ \left(\frac{r_r}{v^- + v^t} - \frac{r_c}{v^+ - v^t} \right) \qquad [1]$$

Supplementary figures

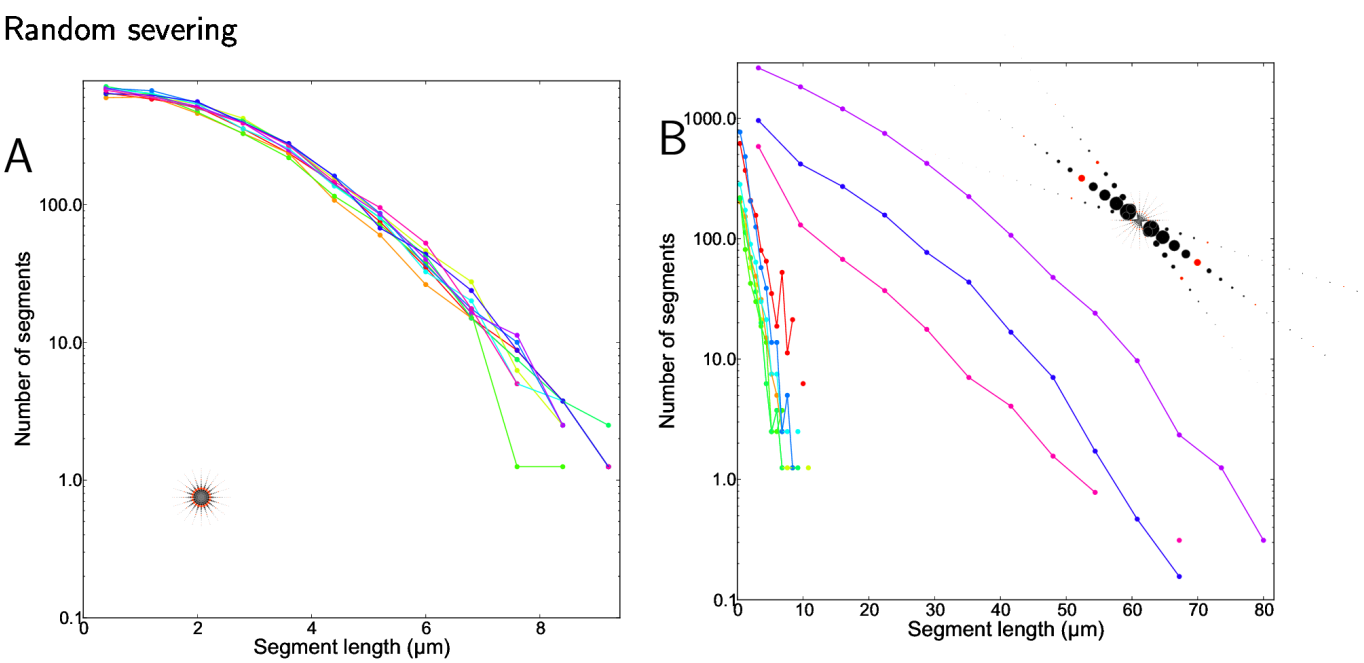

Fig. S1. Example length distributions with random severing. Density of segments with a particular length for 10 equal 18° orientation bins, color coded as in 1E. The y-axis is on a logarithmic scale, so exponential length distributions show as straight lines. A: $r_s = 0.01\ \mu m^{-1}s^{-1}$, $r_x = 0\ s^{-1}$, $r_c = 0.006\ s^{-1}$. B: $r_s = 0.0001\ \mu m^{-1}s^{-1}$, $r_x = 0\ s^{-1}$, $r_c = 0.004\ s^{-1}$. All graphs are averages of ten 3-minute spaced measurements preceding and including 30h. Dotted insets show the orientation of the length histograms with dot surface proportional to the number of segments. All insets are drawn on the same scale.

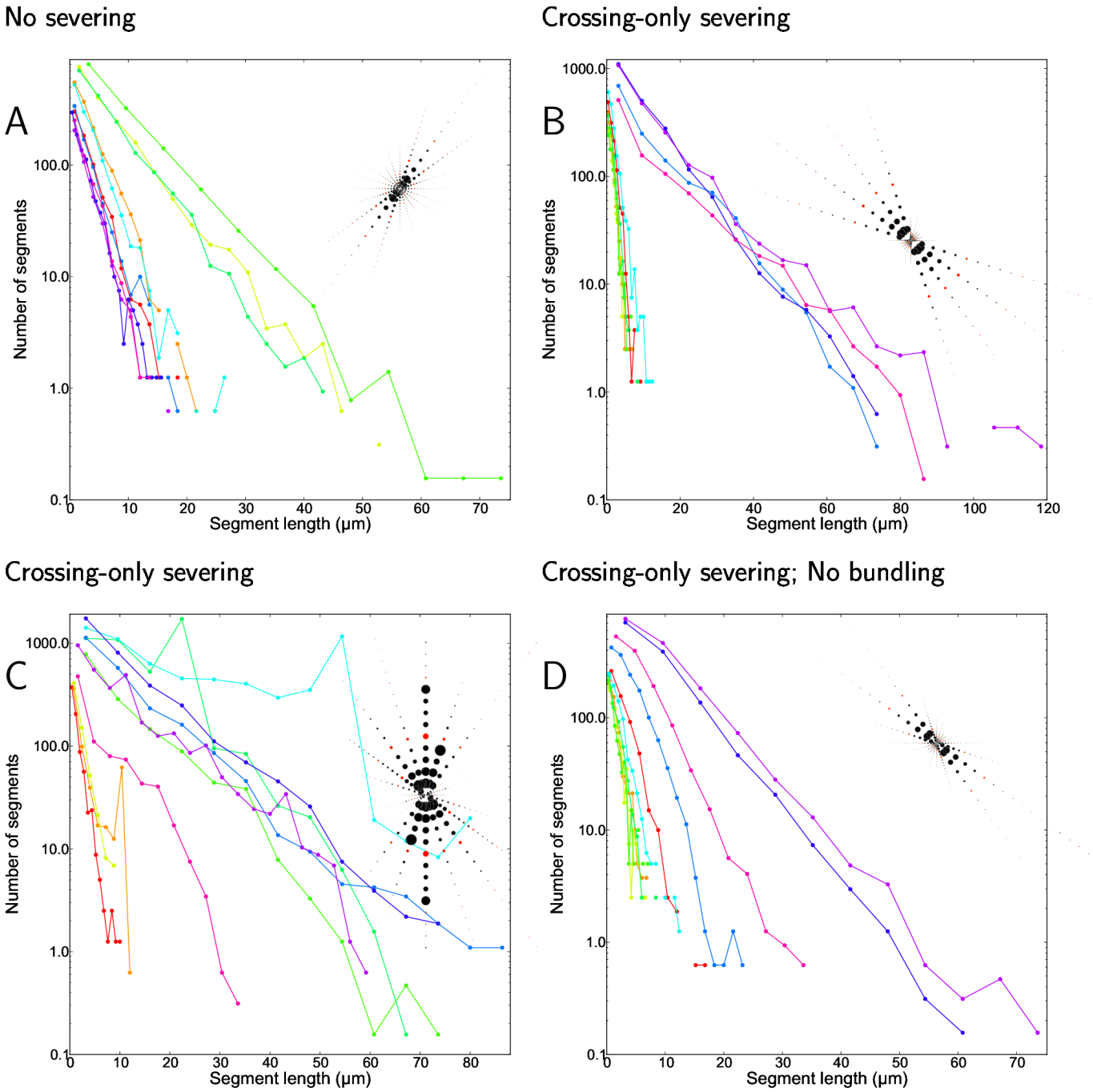

Fig. S2. Example length distributions with no or crossing-only severing. Density of segments with a particular length for 10 equal 18° orientation bins, color coded as in 1E. The y-axis is on a logarithmic scale, so exponential length distributions show as straight lines. A: no severing: $r_s = 0\ \mu m^{-1}s^{-1}$, $r_x = 0\ s^{-1}$, $r_c = 0.006\ s^{-1}$. B: $r_s = 0\ \mu m^{-1}s^{-1}$, $r_x = 0.1\ s^{-1}$, $r_c = 0.006\ s^{-1}$. C: $r_s = 0\ \mu m^{-1}s^{-1}$, $r_x = 0.1\ s^{-1}$, $r_c = 0.004\ s^{-1}$. D: No zippering; $r_s = 0\ \mu m^{-1}s^{-1}$, $r_x = 0.01\ s^{-1}$, $r_c = 0.0035\ s^{-1}$. All graphs are averages of ten 3-minute spaced measurements preceding and including 30h. Dotted insets show the orientation of the length histograms with dot surface proportional to the number of segments. All insets are drawn on the same scale as in fig. S1.

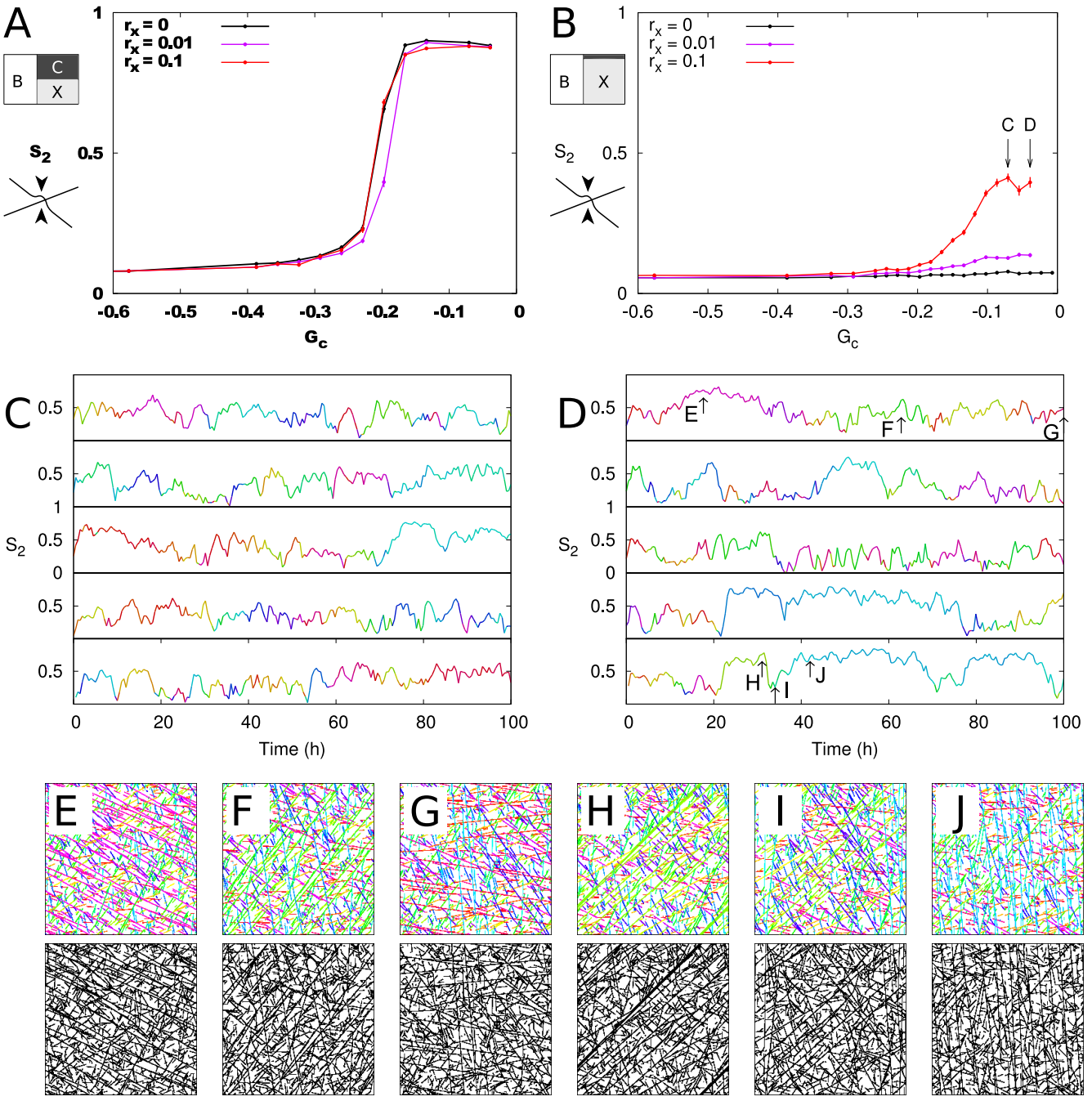

Fig. S3. Aselective severing destabilizes alignment. A,B: severing at crossovers, but randomly selecting the crossed over or crossing MT (bundle) for severing (with bundling). A: $P_{cat} = 0.5$. B: $P_{cat} = 0.09$. Error bars show the SEM with n=100 independent simulations per data point. T=30h. C,D: time traces of S_2 of individual runs from the half-aligned regime of B (up to 100h), colored by array orientation θ_{S_2} on a circular scale as in fig. 1E. $r_x = 0.1\ s^{-1}$, $r_c = 0.004\ s^{-1}$ (C) or $r_c = 0.0035\ s^{-1}$ (D), as indicated with arrows in B. E-J: snapshots of the points indicated with arrows and letters in D.

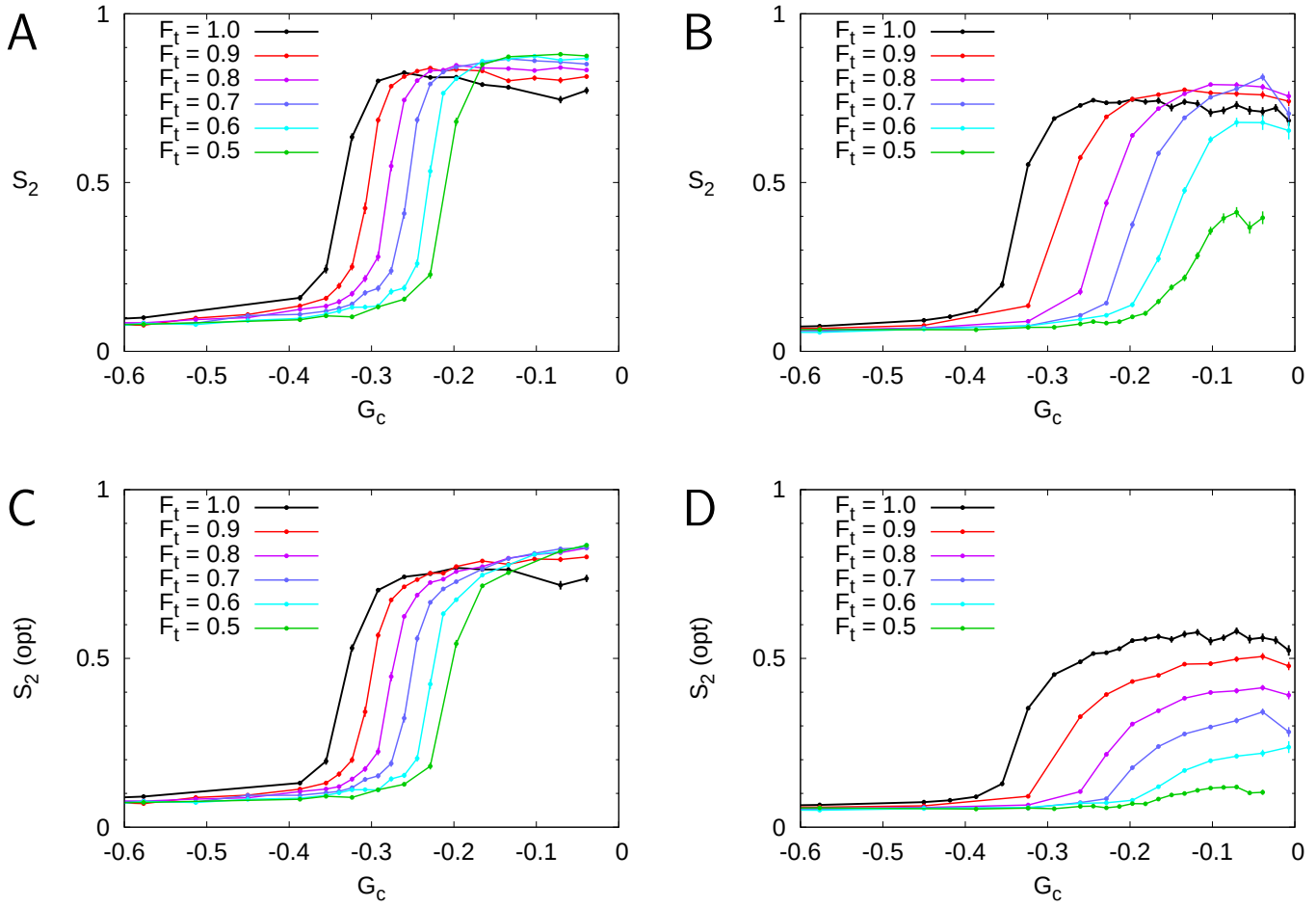

Fig. S4. Transtion between aselective crossover-severing ($F_t = 0.5$) and crossing-only severing ($F_t = 1$) is gradual. At each severing event, severing the crossing MT (bundle) had probability F_t. Figures show G_c, S_2 curves for different values of F_t, as indicated. A,B: regular S_2, C,D: "optical" S_2. A,C: high (default) fraction of induced catastrophes ($F_{ic} = 0.5$), B,D: Low fraction of induced catastrophes ($F_{ic} = 0.09$). $r_x = 0.1\ s^{-1}$. Error bars represent SEM with n=100 independent simulations per data point.

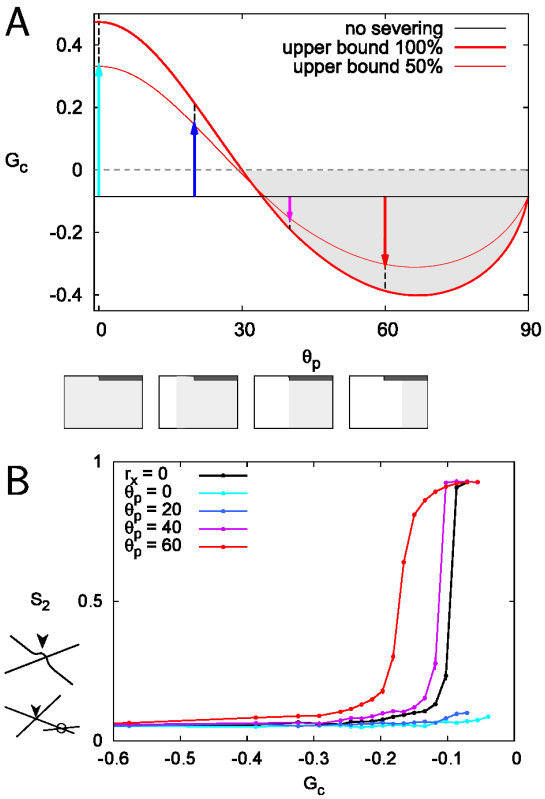

Fig. S5. Bundling normally protects nearly aligned MTs from crossover severing. *As figure 2BC, but with* $P_{cat} = 0.09$ *instead of the default* $P_{cat} = 0.5$. A: The theoretically estimated effect of protecting angles less than θ_p from severing: spontaneous alignment may occur in the gray area ($0 > G_c > G^*$). The thick red curves assume that severing at intersections is equally effective as direct induced catastrophes, which necessarily overestimates their effectiveness to some extent and thus provides an upper bound. The thin red curves show predictions for 50% effectiveness, illustrating the nonlinear approach towards the maximum. The cartoons at the bottom show the interaction functions used for C corresponding to the colored arrows: dark gray represents induced catastrophes, light gray represents crossovers that may be severed later and white crossovers that are protected from severing. B: The negative effect of crossing-only severing on alignment disappears if shallow angles (below $\theta_p = 20, 40, 60^\circ$) are protected from severing and turns into a positive effect for $\theta_p = 40^\circ$and 60°. Error bars represent SEM with n=100 independent simulations per data point.

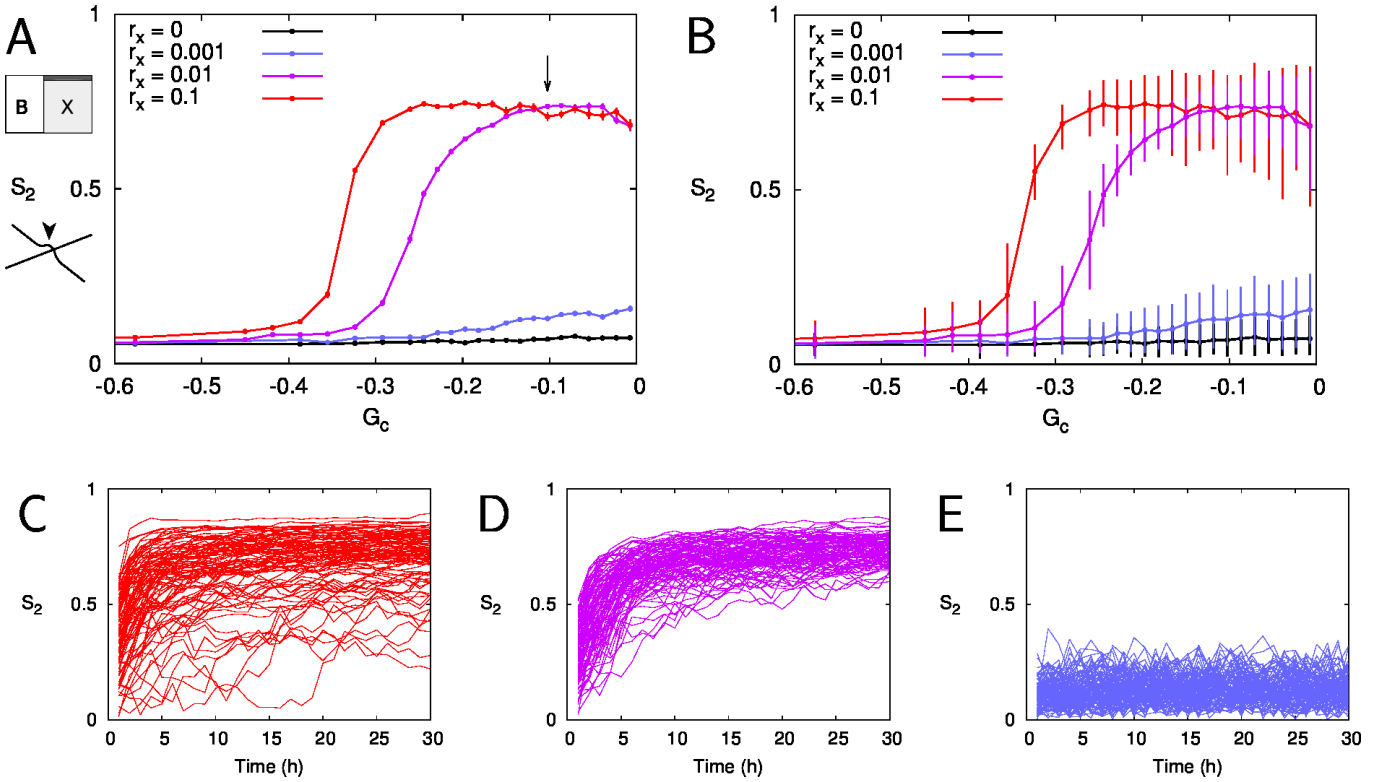

Fig. S6. Crossing-only severing is essential for alignment if induced catastrophes are rare ($P_{cat} = 0.09$). Bundling occurs for $\theta < 40°$. A,B: G_c, S_2 graphs for no severing (black), $r_x = 0.1\ s^{-1}$ (red), $r_x = 0.01\ s^{-1}$ (purple) and $r_x = 0.001\ s^{-1}$ (blue). All points are the average of 100 independent simulations. Error bars indicate SEM (A) or 10-90% intervals of the data (B). C,D,E: S_2-Time traces for all runs at $r_c = 0.0045\ s^{-1}$ ($G_c \approx -0.10$, see arrow in A). C: $r_x = 0.1\ s^{-1}$. D: $r_x = 0.01\ s^{-1}$. E: $r_x = 0.001\ s^{-1}$.

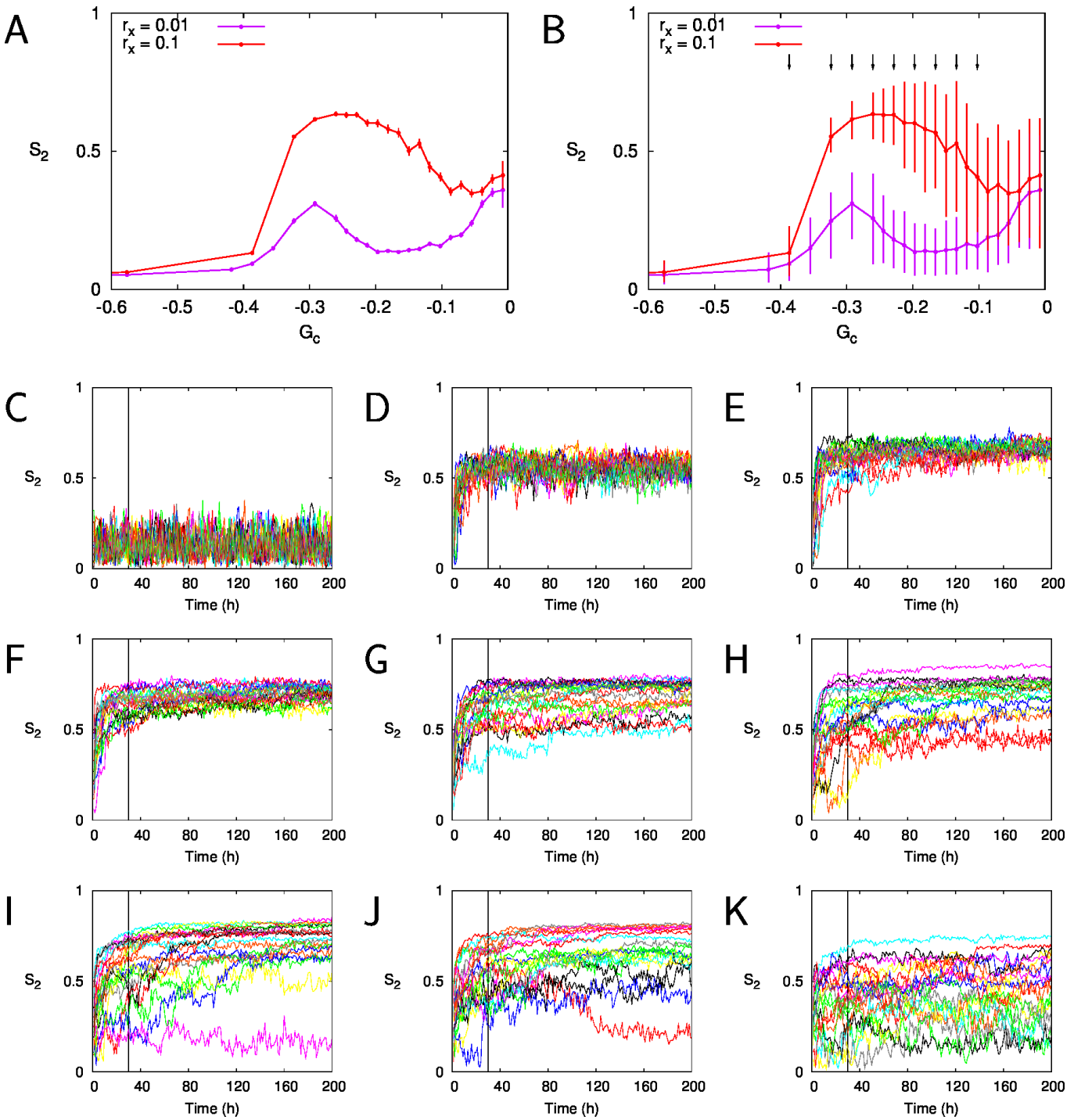

Fig. S7. Crossing-only severing can at best induce a moderate degree of alignment in absence of induced catastrophes ($P_{cat} = 0$), and is more efficient in combination with induced catastrophes A,B: Degree of global alignment S_2 after T=30h. n=100 individual simulations per point. Error bars indicate SEM (A) or 10-90% intervals of the data (B). C-K: Time traces for 200h for 20 independent simulations per parameter combination at the G_c-values indicated with arrows in B. The vertical black line indicates T=30h. All runs: $r_x = 0.1s^{-1}$. C: $r_c = 0.009s^{-1}$ D: $r_c = 0.008s^{-1}$ E: $r_c = 0.0075s^{-1}$ F: $r_c = 0.007s^{-1}$ G: $r_c = 0.0065s^{-1}$ H: $r_c = 0.006s^{-1}$ I: $r_c = 0.0055s^{-1}$ J: $r_c = 0.005s^{-1}$ K: $r_c = 0.0045s^{-1}$. See also fig. S8.

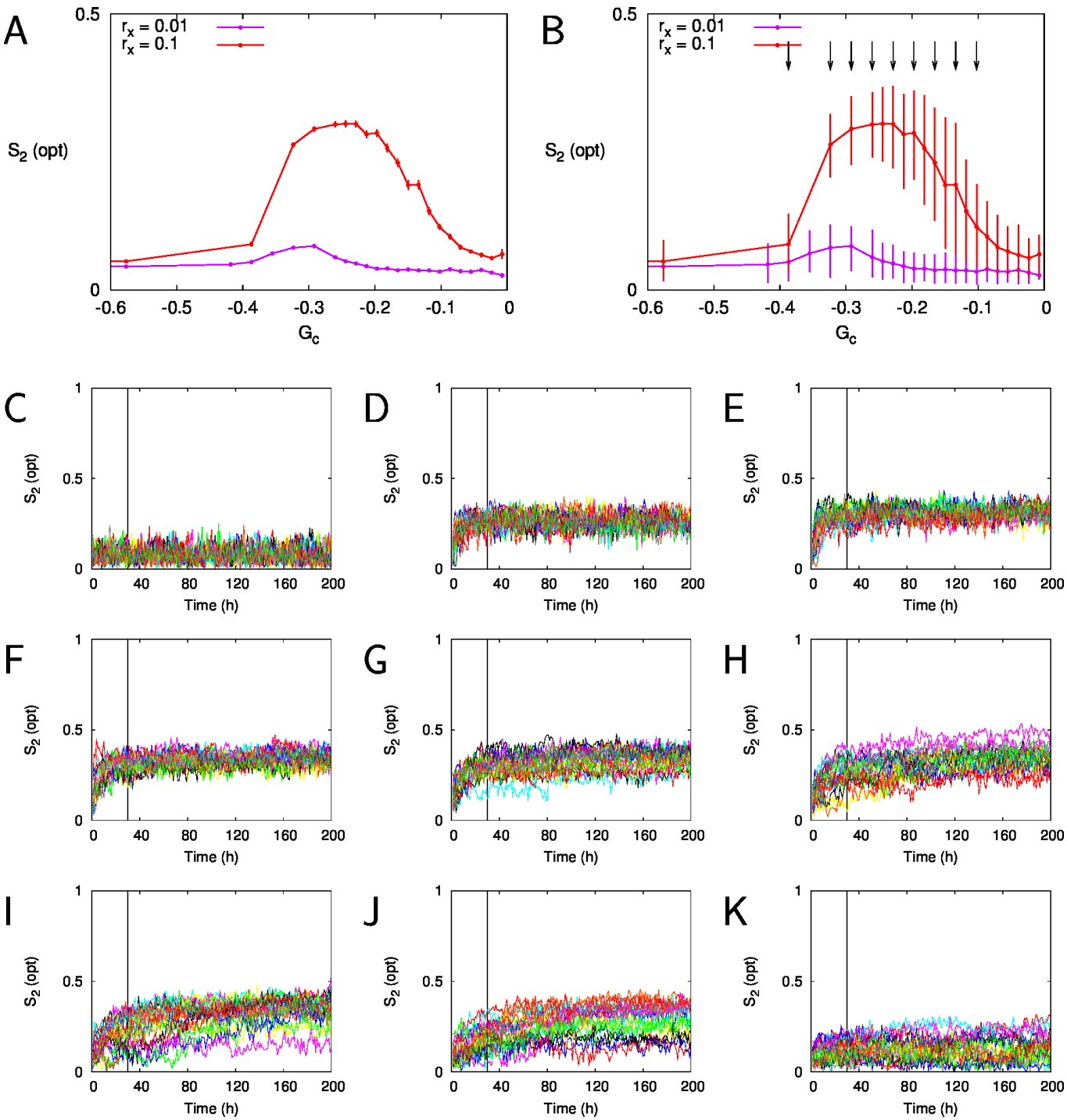

Fig. S8. *As figure S7 (no induced catastrophes; $P_{cat} = 0$), but with "optical" S_2: each bundled stretch of MTs is accounted as a singular MT part.* A,B: Degree of global alignment S_2(optical) after T=30h. n=100 individual simulations per point. Error bars indicate SEM (A) or 10-90% intervals of the data (B). C-K: Time traces for 200h for 20 independent simulations per parameter combination at the G_c-values indicated with arrows in B. The vertical black line indicates T=30h. All runs: $r_x = 0.1s^{-1}$. C: $r_c = 0.009s^{-1}$ D: $r_c = 0.008s^{-1}$ E: $r_c = 0.0075s^{-1}$ F: $r_c = 0.007s^{-1}$ G: $r_c = 0.0065s^{-1}$ H: $r_c = 0.006s^{-1}$ I: $r_c = 0.0055s^{-1}$ J: $r_c = 0.005s^{-1}$ K: $r_c = 0.0045s^{-1}$.

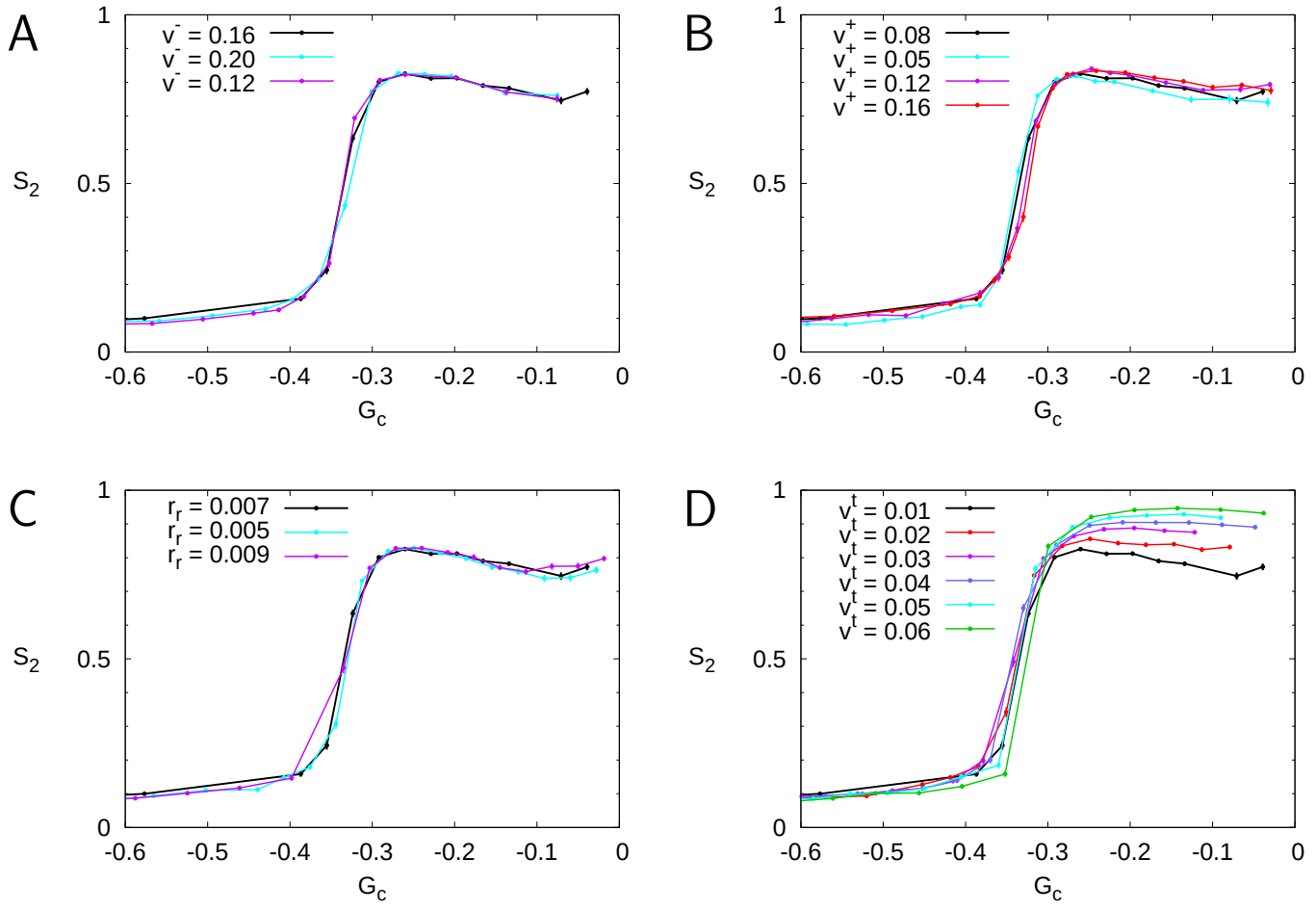

Fig. S9. Changes in MT stability do not affect the boundary (G^*) between disorder and alignment. Black lines indicate default parameter values, other values as indicated in the figures. A: varying v^- (unit: $\mu m/s$), B: varying v^+ (unit: $\mu m/s$), C: varying r_r (unit: s^{-1}), D: varying v^t (unit: $\mu m/s$). All figures: $r_x = 0.1/s$. Error bars indicate SEM of n=100 independent simulations per point. Data at T=30h.

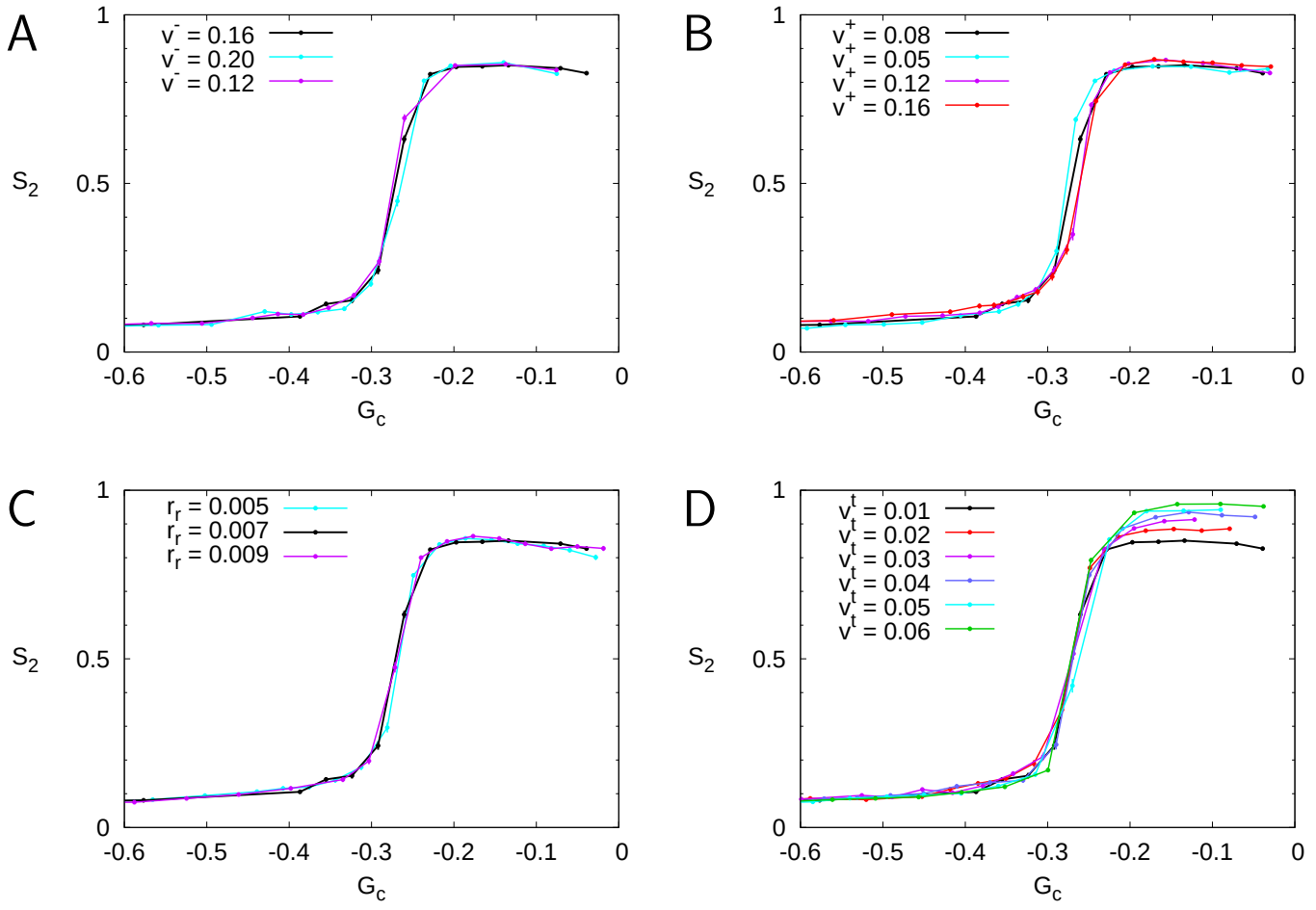

Fig. S10. Changes in MT stability do not affect the boundary (G^*) between disorder and alignment. *Similar to fig. S9, but with $r_x = 0.01/s$.* Black lines indicate default parameter values, other values as indicated in the figures. A: varying v^- (unit: $\mu m/s$), B: varying v^+ (unit: $\mu m/s$), C: varying r_r (unit: s^{-1}), D: varying v^t (unit: $\mu m/s$). All figures: $r_x = 0.01/s$. Error bars indicate SEM of n=100 independent simulations per point. Data at T=30h.

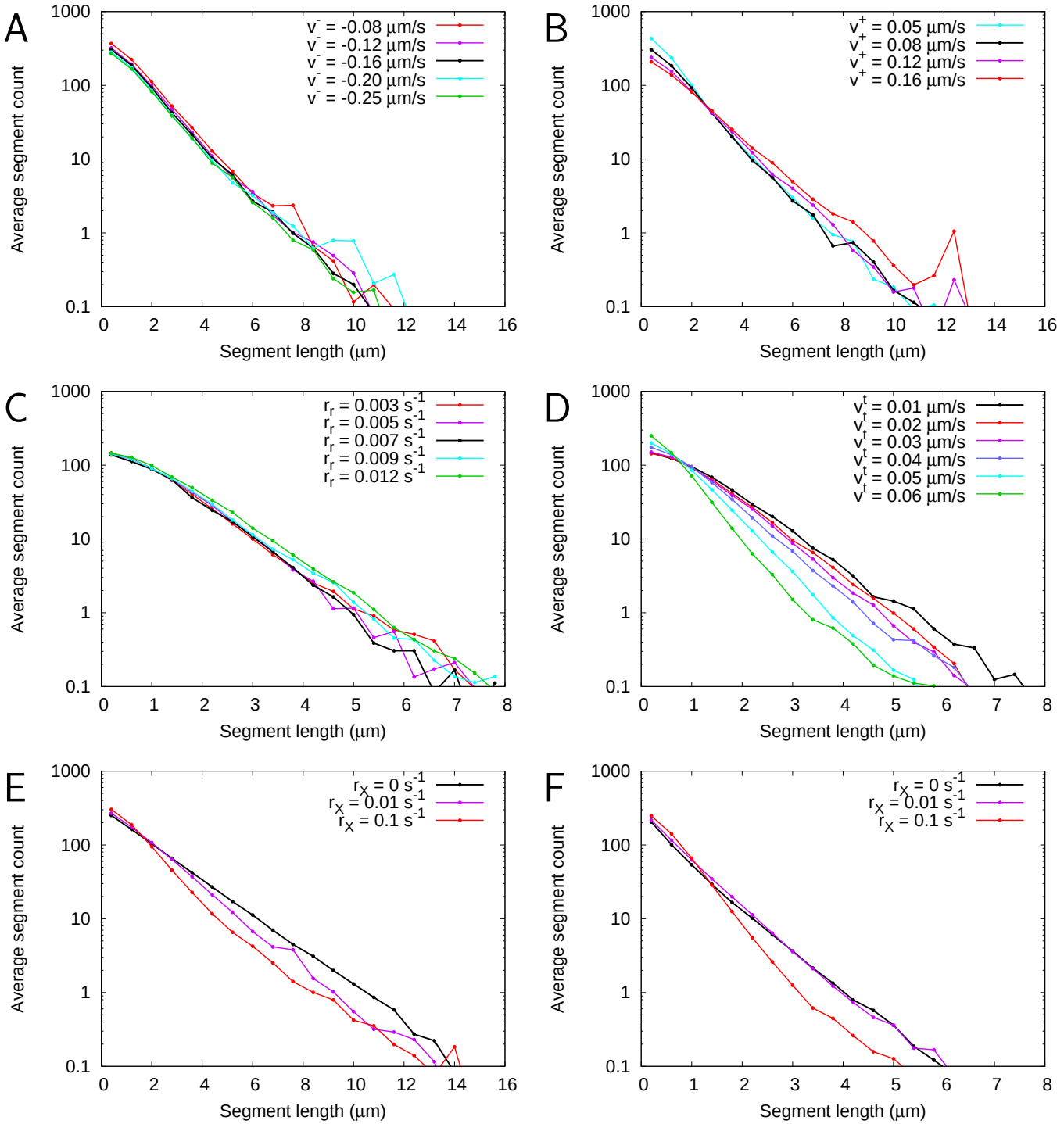

Fig. S11. Changes of length distributions at constant G_c depend on their effect on l_0, the average length of non-interacting MTs. Black lines indicate default parameter values, other values as indicated in the figures. A: varying v^-, B: varying v^+, C: varying r_r, D: varying v^t. E,F: Varying r_x. E: $v^t = 0.01\mu m/s$, F: $v^t = 0.04\mu m/s$. A-D: $r_x = 0.1/s$, n=100 independent simulations per point. Data at T=30h. For effects on l_0, see tables under text T5.

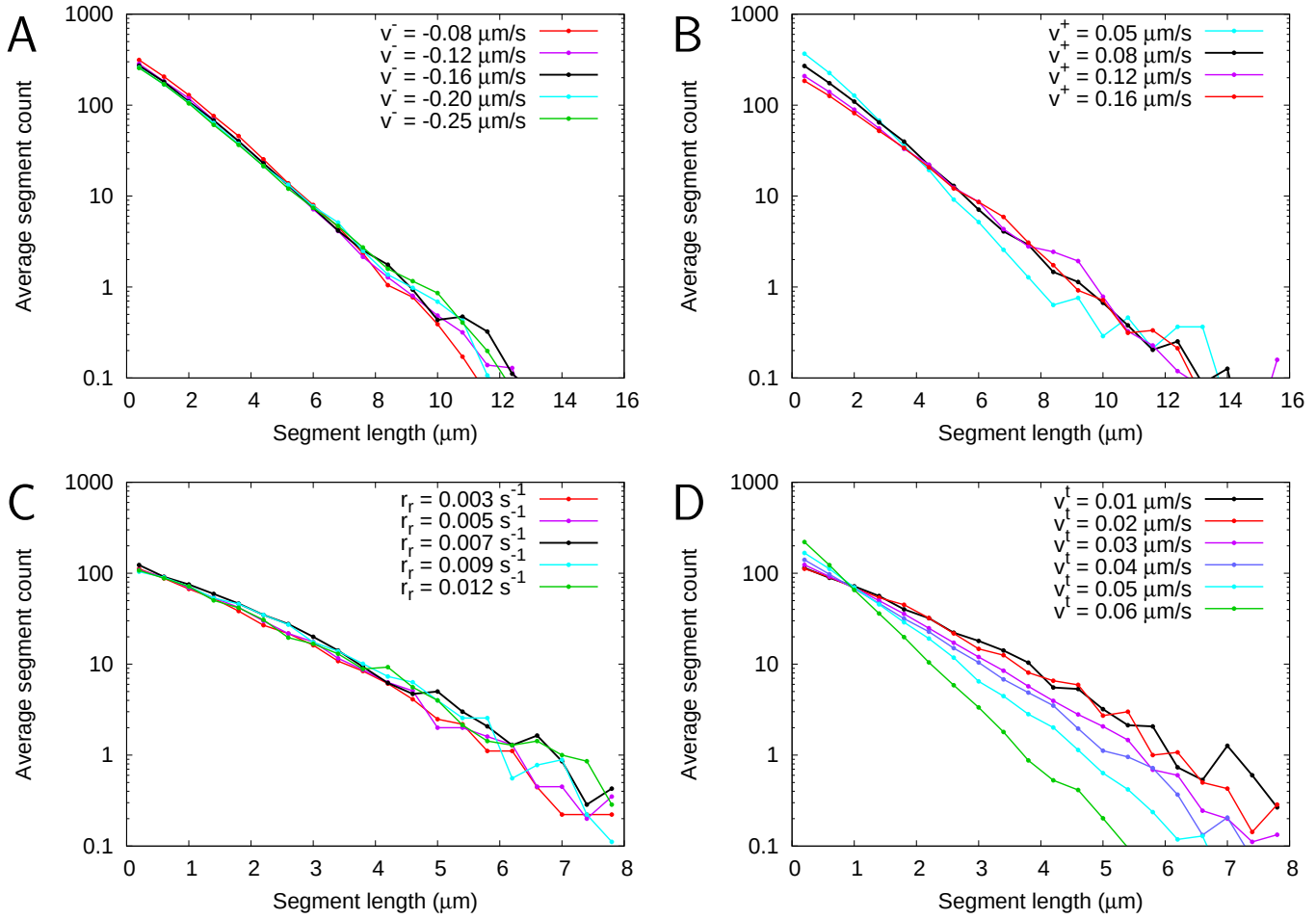

Fig. S12. Changes of length distributions at constant G_c depend on their effect on l_0, the average length of non-interacting MTs. *Similar to fig. S11, but with $r_x = 0.01/s$.* Black lines indicate default parameter values, other values as indicated in the figures. A: varying v^-, B: varying v^+, C: varying r_r, D: varying v^t. All figures: $r_x = 0.01/s$, n=100 independent simulations per point. Data at T=30h. For effects on l_0, see tables under text T5.

Supplementary Tables

Table S1. Overview of parameters.

Parameter	Default	Description
r_s	$0\ \mu\mathrm{m}^{-1}\,\mathrm{s}^{-1}$	Severing rate for random severing (per μm of MT length)
r_x	0 / 0.01 / 0.1 s^{-1}	Severing rate for crossover severing (per crossover)
–	crossing-only	Location of crossover severing: crossing-only or aselective (either side of the crossover)
θ_p	0°	Protected angle for crossover severing: no severing if the relative angle between MTs is $< \theta_p$. Only used in fig. 2
T	30h	Simulated time
v^+	$0.08\ \mu\mathrm{m}\,\mathrm{s}^{-1}$	Growth speed
v^-	$0.16\ \mu\mathrm{m}\,\mathrm{s}^{-1}$	Shrinkage speed
v^t	$0.01\ \mu\mathrm{ms}^{-1}$	Treadmilling speed
r_r	$0.007\ \mathrm{s}^{-1}$	Rescue rate
r_c	variable: 0.003 – $0.010\ \mathrm{s}^{-1}$; default: $0.0045\mathrm{s}^{-1}$	Spontaneous catastrophe rate
r_n	$0.001\ \mathrm{s}^{-1}\,\mu\mathrm{m}^{-2}$	Nucleation rate
θ^*	40°	Maximum bundling angle
P_{cat}	0.5	Induced catastrophe probability (for $\theta > \theta^*$)
$W \times H$	$80 \times 80\ \mu\mathrm{m}$	System size (periodic boundaries)
F_t	1	Fraction of crossover severing events in which the crossing MT (bundle) was selected for severing. Only used explicitly in fig. S4. $F_t = 1$ is the same as crossing-only severing, $F_t = 0.5$ is the same as aselective crossover severing.

Table S2. Short MT abundances based on maximum histogram lengths of 16 μm (top) or 8 μm (bottom).

				$S_2\pm$ SEM			Fraction of MTs shorter than: 0.8 μm	1.6 μm	0.8 μm	1.6 μm	0.8 μm	1.6 μm
		r_c (s^{-1})	l_0 (μm)	$r_x = 0.1$/s	$r_x = 0.01$/s	$r_x = 0$/s	$r_x = 0.1$/s		$r_x = 0.01$/s		$r_x = 0$/s	
v^t	0.01	0.00481	36.4	0.75 ± 0.012	0.86 ± 0.004	0.90 ± 0.003	0.44	0.72	0.38	0.63	0.36	0.59
	0.02	0.00413	33.4	0.84 ± 0.005	0.88 ± 0.004	0.92 ± 0.003	0.46	0.74	0.38	0.63	0.38	0.62
	0.03	0.00350	30.2	0.87 ± 0.005	0.92 ± 0.004	0.94 ± 0.003	0.49	0.77	0.42	0.67	0.42	0.66
	0.04	0.00291	26.4	0.91 ± 0.004	0.93 ± 0.004	0.95 ± 0.003	0.54	0.81	0.47	0.72	0.47	0.71
	0.05	0.00235	22.2	0.92 ± 0.004	0.95 ± 0.003	0.96 ± 0.003	0.61	0.86	0.55	0.80	0.56	0.78
	0.06	0.00180	17.2	0.95 ± 0.003	0.96 ± 0.003	0.97 ± 0.003	0.72	0.92	0.66	0.87	0.66	0.86
v^-	0.08	0.00752	33.8	0.77 ± 0.010	0.85 ± 0.005	–	0.45	0.72	0.38	0.63	–	–
	0.12	0.00574	35.5	0.77 ± 0.010	0.84 ± 0.005	–	0.45	0.72	0.39	0.63	–	–
	0.16	0.00480	36.5	0.77 ± 0.010	0.85 ± 0.005	–	0.45	0.72	0.38	0.63	–	–
	0.20	0.00421	37.2	0.76 ± 0.010	0.84 ± 0.004	–	0.45	0.72	0.38	0.63	–	–
	0.25	0.00374	37.8	0.76 ± 0.009	0.85 ± 0.005	–	0.45	0.72	0.38	0.63	–	–
v^+	0.05	0.00295	30.7	0.75 ± 0.012	0.84 ± 0.006	–	0.50	0.78	0.42	0.68	–	–
	0.08	0.00480	36.5	0.76 ± 0.011	0.84 ± 0.006	–	0.45	0.73	0.38	0.63	–	–
	0.12	0.00722	40.9	0.78 ± 0.008	0.86 ± 0.004	–	0.42	0.68	0.36	0.60	–	–
	0.16	0.00960	43.7	0.79 ± 0.007	0.86 ± 0.005	–	0.40	0.66	0.35	0.58	–	–
r_r	0.003	0.00315	36.5	0.75 ± 0.011	0.83 ± 0.005	–	0.46	0.73	0.40	0.64	–	–
	0.005	0.00398	36.5	0.77 ± 0.008	0.84 ± 0.006	–	0.45	0.73	0.39	0.64	–	–
	0.007	0.00480	36.5	0.77 ± 0.010	0.85 ± 0.004	–	0.44	0.71	0.38	0.63	–	–
	0.009	0.00562	36.5	0.77 ± 0.008	0.85 ± 0.005	–	0.44	0.72	0.37	0.62	–	–
	0.012	0.00686	36.5	0.78 ± 0.010	0.85 ± 0.005	–	0.43	0.71	0.37	0.61	–	–

				$S_2\pm$ SEM			Fraction of MTs shorter than: 0.8 μm	1.6 μm	0.8 μm	1.6 μm	0.8 μm	1.6 μm
		r_c (s^{-1})	l_0 (μm)	$r_x = 0.1$/s	$r_x = 0.01$/s	$r_x = 0$/s	$r_x = 0.1$/s		$r_x = 0.01$/s		$r_x = 0$/s	
v^t	0.01	0.00481	36.4	0.75 ± 0.012	0.86 ± 0.004	0.90 ± 0.003	0.48	0.77	0.42	0.68	0.41	0.66
	0.02	0.00413	33.4	0.84 ± 0.005	0.88 ± 0.004	0.92 ± 0.003	0.49	0.78	0.42	0.68	0.47	0.71
	0.03	0.00350	30.2	0.87 ± 0.005	0.92 ± 0.004	0.94 ± 0.003	0.52	0.81	0.46	0.73	0.50	0.75
	0.04	0.00291	26.4	0.91 ± 0.004	0.93 ± 0.004	0.95 ± 0.003	0.58	0.86	0.52	0.77	0.56	0.80
	0.05	0.00235	22.2	0.92 ± 0.004	0.95 ± 0.003	0.96 ± 0.003	0.65	0.90	0.59	0.83	0.64	0.86
	0.06	0.00180	17.2	0.95 ± 0.003	0.96 ± 0.003	0.97 ± 0.003	0.77	0.95	0.70	0.90	0.71	0.90
v^-	0.08	0.00752	33.8	0.77 ± 0.010	0.85 ± 0.005	–	0.49	0.78	0.42	0.68	–	–
	0.12	0.00574	35.5	0.77 ± 0.010	0.84 ± 0.005	–	0.49	0.78	0.41	0.67	–	–
	0.16	0.00480	36.5	0.77 ± 0.010	0.85 ± 0.005	–	0.49	0.77	0.42	0.68	–	–
	0.20	0.00421	37.2	0.76 ± 0.010	0.84 ± 0.004	–	0.48	0.77	0.41	0.67	–	–
	0.25	0.00374	37.8	0.76 ± 0.009	0.85 ± 0.005	–	0.49	0.78	0.41	0.67	–	–
v^+	0.05	0.00295	30.7	0.75 ± 0.012	0.84 ± 0.006	–	–	–	–	–	–	–
	0.08	0.00480	36.5	0.76 ± 0.011	0.84 ± 0.006	–	–	–	–	–	–	–
	0.12	0.00722	40.9	0.78 ± 0.008	0.86 ± 0.004	–	–	–	–	–	–	–
	0.16	0.00960	43.7	0.79 ± 0.007	0.86 ± 0.005	–	–	–	–	–	–	–
r_r	0.003	0.00315	36.5	0.75 ± 0.011	0.83 ± 0.005	–	0.50	0.79	0.43	0.69	–	–
	0.005	0.00398	36.5	0.77 ± 0.008	0.84 ± 0.006	–	0.49	0.78	0.42	0.68	–	–
	0.007	0.00480	36.5	0.77 ± 0.010	0.85 ± 0.004	–	0.48	0.78	0.41	0.67	–	–
	0.009	0.00562	36.5	0.77 ± 0.008	0.85 ± 0.005	–	0.48	0.77	0.40	0.66	–	–
	0.012	0.00686	36.5	0.78 ± 0.010	0.85 ± 0.005	–	0.47	0.76	0.40	0.66	–	–

References

1. Lindeboom JJ, et al. (2013) Cortical microtubule arrays are initiated from a nonrandom prepattern driven by atypical microtubule initiation. *Plant Physiol* 161(3):1189–1201.
2. Tindemans SH, Deinum EE, Lindeboom JJ, Mulder B (2014) Efficient event-driven simulations shed new light on microtubule organisation in the plant cortical array. *Frontiers in Physics* 2(19):9.
3. Dogterom M, Leibler S (1993) Physical aspects of the growth and regulation of microtubule structures. *Physical Review Letters* 70(9):1347–1350.
4. Hawkins RJ, Tindemans SH, Mulder BM (2010) Model for the orientational ordering of the plant microtubule cortical array. *Physical review. E, Statistical, nonlinear, and soft matter physics* 82(1 Pt 1):011911.
5. Tindemans SH, Mulder BM (2010) Microtubule length distributions in the presence of protein-induced severing. *Phys Rev E Stat Nonlin Soft Matter Phys* 81(3 Pt 1):031910.
6. Deinum EE (2013) Ph.D. thesis.